Spilling breakers : applications to Favre waves and to the shoaling and the breaking of the solitary wave

Sergey L. Gavrilyuk, Valery Liapidevskii, Alexander Chesnokov

Spilling breakers : applications to Favre waves and to the shoaling and the breaking of the solitary wave

S. L. Gavrilyuk*, V. Yu. Liapidevskii†, A. A. Chesnokov‡

January 28, 2016

Abstract

A two-layer long wave approximation of the homogeneous Euler equations for a free surface flow over a rigid bottom is derived. The upper layer is turbulent and is described by depth averaged equations for the layer thickness, the average fluid velocity inside the layer, and the fluid turbulent energy. The lower layer is almost potential and can be described by Serre–Su–Gardner–Green–Naghdi equations (second order shallow water approximation with respect to the parameter H/L where H is a characteristic water depth, and L is a characteristic wave length). The interaction between the layers is due to the turbulent mixing. The dynamics of the interface separating two layers is governed by the turbulent energy of the upper layer. Stationary supercritical solutions to this model are first constructed, containing, in particular, a local subcritical zone at the forward slope of the wave. Such a local subcritical zone corresponds to an intense increasing of a turbulent layer thickness and can thus be associated with the spilling breaker formation.

Non-stationary model was then numerically solved and compared with experimental data for the following two problems. The first one is the study of surface waves resulting from the interaction of a uniform free surface fluid flow with an immobile wall ('the water hammer problem with a free surface'). These waves are sometimes called 'Favre waves' in homage to Henry Favre and his contribution to the study of this phenomena. When the Froude number is between 1 and approximately 1.3, the undular bore appears. The turbulent energy of the flow is localized at the wave

*Corresponding author, Aix-Marseille Université, UMR CNRS 7343, IUSTI, 5 rue E. Fermi, 13453 Marseille CEDEX 13, France and Novosibirsk State University, 2 Pirogova street, 630090 Novosibirsk, Russia, sergey.gavrilyuk@univ-amu.fr

†Lavrentyev Institute of Hydrodynamics, 15 Lavrentyev prospect, 630090 Novosibirsk, and Novosibirsk State University, 2 Pirogova street, 630090 Novosibirsk, Russia, liapid@hydro.nsc.ru

‡Lavrentyev Institute of Hydrodynamics, 15 Lavrentyev prospect, 630090 Novosibirsk, and Novosibirsk State University, 2 Pirogova street, 630090 Novosibirsk, Russia, chesnokov@hydro.nsc.ru

crests. The characteristics of the leading wave are in good agreement with the experimental data by Favre (1935) and Treske (1994). When the Froude number is between 1.3 and 1.4, the transition from the undular bore to the breaking (monotone) bore occurs. In the breaking bore, the turbulent energy is localized at the front of the bore.

The shoaling and the breaking of the solitary wave propagating in a mild - slope (1/60) long channel (300 m) was then studied. Comparison with the experimental data by Hsiao *et.al.* (2008) show a very good agreement of the wave profile evolution.

1 Introduction

If a wave approaching the coast is long and the variation of the coastal slope is gradual, spilling breakers usually appear. They are characterized by the appearance of a finite turbulent fluid zone riding down the forward slope of the wave (Longuet–Higgins & Turner, 1974, Duncan, 2001). At the toe of this turbulent zone the wave slope changes sharply, resulting to the flow separation and the vorticity creation. The breaking waves entrain the air into the water by forming 'whitecaps' where an intensive dissipation occurs. Such a turbulent zone has a strong influence on the wave evolution.

As it was mentioned in Duncan (2011), theoretical models of spilling breakers are rare. Indeed, beyond the multiphase aspects, the modelling depends crucially on a precise description of the flow structure. In the case where the flow potentiality is supposed, one actually uses an interesting approach based on a coupling between the dispersive Green–Naghdi equations describing waves far from the coast, and the hyperbolic Saint–Venant equations near the coast (cf. Tissier *et al.* (2012)). The difficulty is to understand when we replace one model by another one. A search of such a 'switching criteria' is not a well defined problem even if several empirical criteria were proposed in the literature (wave phase velocity becomes larger than the flow velocity, or the wave slope attains a critical value, for example).

In this paper, we will focus only on the turbulence generation in breaking waves without taking into account the multiphase aspects. The difficulties related to the multiphase description of the wave breaking were discussed in details in Brocchini & Peregrine (2001 a,b). The presence of the roller riding the front face of the wave suggests that it is natural to consider vortex flows (shear flows) for deriving an adequate mathematical model for the wave breaking. The main issue of our work is a two-layer modelling, where the upper turbulent layer is considered within the framework of shear shallow water flows (cf. Teshukov, 2007, Richard & Gavrilyuk, 2012, 2013, Castro & Lannes, 2014), while the lower layer is potential and can be described by a Serre–Su–Gardner– Green–Naghdi type model. The interaction between layers is taken into account through a natural mixing process, where the mixing velocity is proportional to the intensity of large eddies of the upper layer. Experimental data on the structure of the turbulent flow field under breaking waves show that the frontiers between the turbulent region caused by the wave breaking and the potential region are

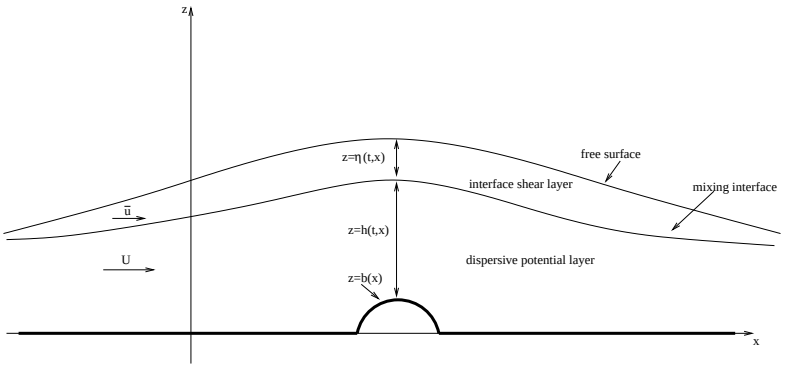

Figure 1: Two-layer flow over topography.

clearly visible (Nadaoka *et al.* 1989, Lin & Rockwell, 1994). This justifies a two-layer scheme for the modelling of the breaking waves. The model generalizes that derived in Liapidevskii & Chesnokov (2014) where the hydrostatic approximation in both layers was used, and that in Richard & Gavrilyuk (2015) where such a two-layer approach was used in the limit where the thickness of the upper shear layer was vanishing.

In section 2 we derive depth-averaged equations. In section 3 stationary solutions are studied. Favre waves and the shoaling and the breaking of the solitary waves are studied in section 4. Technical details are presented in the Appendixes.

2 Two-layer flow over a flat bottom

The simplest model for spilling breakers, without taking into account bubble air trapping, should necessarily deal with a two-layer description of interacting fluid layers: the upper turbulent layer and the lower almost potential layer (see Figure 1). First, we will derive such a two-layer model for flows over a flat bottom.

Consider the Euler equations for two-dimensional flows: in the horizontal direction Ox the component of the velocity is u, and in the vertical direction Oz the velocity component is w. With ρ being the fluid density, and p being the fluid pressure, the Euler equations can be written as :

$$\frac{\partial u}{\partial x} + \frac{\partial w}{\partial z} = 0, \tag{1}$$

$$\rho\left(\frac{\partial u}{\partial t} + u\frac{\partial u}{\partial x} + w\frac{\partial u}{\partial z}\right) = -\frac{\partial p}{\partial x}, \tag{2}$$

$$\rho\left(\frac{\partial w}{\partial t} + u\frac{\partial w}{\partial x} + w\frac{\partial w}{\partial z}\right) = -\rho g - \frac{\partial p}{\partial z}. \tag{3}$$

Here g is the gravity acceleration in the vertical direction. The kinematic boundary condition at $z = 0$ is :

$$w\big|_{z=0} = 0. \tag{4}$$

At the internal boundary $z = h(t, x)$ separating the lower layer where the flow is potential, and the upper turbulent layer, the kinematic condition is :

$$w\big|_{z=h} - \frac{\partial h}{\partial t} - u\big|_{z=h} \frac{\partial h}{\partial x} = M. \tag{5}$$

Here the right hand side M is responsible for the mixing between layers (a formula for M will be proposed later). At the free boundary $z = h(t, x)+\eta(t, x)$ we suppose that

$$w\big|_{z=h+\eta} - \frac{\partial}{\partial t}(h+\eta) - u\big|_{z=h+\eta} \frac{\partial}{\partial x}(h+\eta) = 0, \quad p\big|_{z=h+\eta} = 0. \tag{6}$$

We introduce a classical scaling of the shallow water theory :

$$x \to Lx, \quad z \to Hz, \quad t \to \frac{L}{\sqrt{gH}}t, \quad u \to \sqrt{gH}u,$$
$$w \to \frac{H}{L}\sqrt{gH}w, \quad p \to \rho g H p, \quad h \to Hh.$$

Here H is the characteristic vertical scale, and L is the characteristic horizontal scale. We suppose that the waves are long, so the dimensionless parameter $\varepsilon = H/L$ is small. The equations (1), (2), (3) are transformed into dimensionless form where the corresponding dimensionless variables are denoted by the same letters:

$$\frac{\partial u}{\partial x} + \frac{\partial w}{\partial z} = 0, \tag{7}$$

$$\frac{\partial u}{\partial t} + \frac{\partial u^2}{\partial x} + \frac{\partial uw}{\partial z} = -\frac{\partial p}{\partial x}, \tag{8}$$

$$\varepsilon^2\left(\frac{\partial w}{\partial t} + \frac{\partial uw}{\partial x} + \frac{\partial w^2}{\partial z}\right) = -\left(1 + \frac{\partial p}{\partial z}\right). \tag{9}$$

Equations (7), (8), (9) admit the conservation of energy:

$$\frac{\partial E}{\partial t} + \frac{\partial}{\partial x}(uE + pu) + \frac{\partial}{\partial z}(wE + pw) = 0 \tag{10}$$

where

$$E = \frac{u^2}{2} + \varepsilon^2\frac{w^2}{2} + z$$

is the dimensionless specific energy.

2.1 Depth-averaged equations for the lower potential layer

Integrating the incompressibility, the horizontal momentum and the energy equations with respect to z over the fluid depth and using the boundary conditions (4), (5), we obtain the following exact integral relations for the lower layer:

$$\frac{\partial h}{\partial t} + \frac{\partial}{\partial x}\left(\int_0^h u\, dz \right) = -M, \tag{11}$$

$$\frac{\partial}{\partial t}\left(\int_0^h u\, dz \right) + \frac{\partial}{\partial x}\left(\int_0^h u^2\, dz + \int_0^h p\, dz \right) = p\big|_{z=h} h_x - Mu\big|_{z=h}, \tag{12}$$

$$\frac{\partial}{\partial t}\left(\int_0^h \left(\frac{u^2}{2} + \varepsilon^2 \frac{w^2}{2} + z \right) dz \right) + \frac{\partial}{\partial x}\left(\int_0^h u\left(\frac{u^2}{2} + \varepsilon^2 \frac{w^2}{2} + z \right) dz + \int_0^h pu\, dz \right)$$
$$= -p\big|_{z=h}(h_t + M) - M\left(\frac{u^2}{2} + \varepsilon^2 \frac{w^2}{2} + h \right)\Big|_{z=h}. \tag{13}$$

Introducing the average velocity in the lower layer

$$U = \frac{1}{h}\int_0^h u\, dz$$

we can rewrite the conservation of the mass in the following form:

$$\frac{\partial h}{\partial t} + \frac{\partial}{\partial x}(hU) = -M.$$

To obtain a closed system of governing equation, we need to know the pressure distribution in the layer. Integrating the equation (1) from 0 to z, $0 < z < h(t,x)$ we obtain

$$w(t,x,z) = -\int_0^z u_x(t,x,s)\, ds.$$

In zero order with respect to ε, the vertical velocity is

$$w(t,x,z) \approx -U_x z. \tag{14}$$

A second order approximation for the pressure comes from (9) where we have to replace w by (14):

$$\frac{\partial p}{\partial z} \approx -1 - \varepsilon^2 \left(\frac{\partial w}{\partial t} + u\frac{\partial w}{\partial x} + w\frac{\partial w}{\partial z} \right) \approx -1 + \varepsilon^2 z \left(U_{xt} + UU_{xx} - U_x^2 \right).$$

Integrating it from h to z $(0 < z < h)$ we obtain

$$p \approx p\big|_{z=h} - (z-h) + \varepsilon^2 \left(U_{xt} + UU_{xx} - U_x^2 \right) \frac{z^2 - h^2}{2}.$$

The integral of the pressure can thus be evaluated:

$$\int_0^h p\, dz \approx p\big|_{z=h}\, h + \frac{h^2}{2} - \varepsilon^2 \frac{h^3}{3}\left(U_{xt} + UU_{xx} - U_x^2 \right).$$

One can also prove that if the flow is weakly sheared, i.e. the dimensionless flow vorticity $\omega = u_z - \varepsilon^2 w_x = O\left(\varepsilon^\beta\right)$ with $1 < \beta \leq 2$ then

$$\int_0^h u^2\, dz = hU^2 + O\left(\varepsilon^{2\beta}\right) \tag{15}$$

(see for the proof Barros *et al.* 2007 or Gavrilyuk *et al.* 2015). In particular, in the potential case $\beta = 2$. Analogous estimation of integrals can be given for the energy equation. Keeping only terms of order one and ε^2, we obtain the final system for a lower potential layer with mixing at the interface $z = h(t,x)$:

$$\frac{\partial h}{\partial t} + \frac{\partial}{\partial x}(hU) = -M,$$

$$\frac{\partial}{\partial t}(hU) + \frac{\partial}{\partial x}\left(hU^2 + \int_0^h p\, dz\right) = p\big|_{z=h}\, h_x - Mu\big|_{z=h},$$

$$\frac{\partial}{\partial t}\left(h\left(\frac{U^2}{2} + \varepsilon^2\frac{U_x^2}{6}h^2 + \frac{h}{2}\right)\right) + \frac{\partial}{\partial x}\left(hU\left(\frac{U^2}{2} + \varepsilon^2\frac{U_x^2}{6}h^2 + \frac{h}{2}\right) + U\int_0^h p\, dz\right)$$
$$= -p\big|_{z=h}(h_t + M) - M\left(\frac{u^2}{2} + \varepsilon^2\frac{U_x^2h^2}{2} + h\right)\Big|_{z=h},$$

where

$$\int_0^h p\, dz = p\big|_{z=h}\, h + \frac{h^2}{2} - \varepsilon^2\frac{h^3}{3}\left(U_{xt} + UU_{xx} - U_x^2\right).$$

The value of the velocity $u\big|_{z=h}$ is not yet determined. Let us remark that we have formally three governing equations for only two unknowns h and U. The compatibility condition between the energy equation and the momentum and mass equation gives us only one possibility (see Appendix A for the proof):

$$u\big|_{z=h} = U.$$

2.2 Depth-averaged equations for the upper turbulent layer

Consider the following hydrostatic equations in the upper layer having the same density as the lower layer. In dimensionless variables the equations are

$$\frac{\partial u}{\partial x} + \frac{\partial w}{\partial z} = 0,$$

$$\frac{\partial u}{\partial t} + \frac{\partial u^2}{\partial x} + \frac{\partial uw}{\partial z} = -\frac{\partial p}{\partial x}, \quad p(t,x,z) = h + \eta - z.$$

The hydrostatic distribution of the pressure takes already into account the dynamic condition at the free surface. They admit the energy conservation law

$$\frac{\partial}{\partial t}\left(\frac{u^2}{2} + z\right) + \frac{\partial}{\partial x}\left(u\left(\frac{u^2}{2} + z\right) + pu\right) + \frac{\partial}{\partial z}\left(w\left(\frac{u^2}{2} + z\right) + pw\right) = 0.$$

The corresponding kinematic boundary conditions at the free surface and at the internal surface are

$$\frac{\partial}{\partial t}(h+\eta)+u\frac{\partial}{\partial x}(h+\eta)-w\Big|_{z=h+\eta}=0,\quad \frac{\partial h}{\partial t}+u\frac{\partial h}{\partial x}-w\Big|_{z=h}=-M.$$

Averaging the incompressibility equation we obtain :

$$\frac{\partial}{\partial t}\eta+\frac{\partial}{\partial x}(\eta\bar{u})=M,$$

with

$$\bar{u}(t,x)=\frac{1}{\eta}\int_h^{h+\eta}u(t,x,s)\,ds.$$

Averaging of the horizontal momentum equation gives us

$$\frac{\partial}{\partial t}\Big(\int_h^{h+\eta}u\,dz\Big)+\frac{\partial}{\partial x}\Big(\int_h^{h+\eta}(u^2+p)\,dz\Big)=M\,u\big|_{z=h}-p\big|_{z=h}\,h_x,$$

or

$$\frac{\partial}{\partial t}(\eta\bar{u})+\frac{\partial}{\partial x}\Big(\eta\bar{u}^2+\eta e+\frac{\eta^2}{2}\Big)=M\,u\big|_{z=h}-p\big|_{z=h}\,h_x,$$

with the specific turbulent energy e defined as

$$e=\frac{1}{\eta}\int_h^{h+\eta}(u-U)^2\,dz.$$

The averaged energy equation is

$$\frac{\partial}{\partial t}\Big(\int_h^{h+\eta}\Big(\frac{u^2}{2}+z\Big)\,dz\Big)+\frac{\partial}{\partial x}\Big(\int_h^{h+\eta}\Big(u\Big(\frac{u^2}{2}+z\Big)+pu\Big)\,dz\Big)$$

$$=M\Big(\frac{u^2}{2}\Big|_{z=h}+h\Big)+p\big|_{z=h}(h_t+M).$$

We suppose that the shear effects in the upper layer are now more important. More exactly, let the dimensionless flow vorticity $\omega=u_z-\varepsilon^2 w_x\approx u_z=O(\varepsilon^\beta)$ with $0<\beta<1$ (so, $u_z=O(\varepsilon^\beta)$). Then

$$\int_0^h(u-U)^2\,dz=O\left(\varepsilon^{2\beta}\right). \tag{16}$$

This term is now more important than the dispersion which is of order ε^2, and should be kept in the momentum equation. The vorticity is 'weak' in the sense that it is not of order one, but it could be 'large' at the same time ('almost'

of order one) when β is small. Analogous estimation of integrals can be given for the energy equation (see Teshukov, 2007; Richard & Gavrilyuk, 2012, 2013 for details). Keeping only terms of order one and $\varepsilon^{2\beta}$, we obtain the energy equation for the lower potential layer in the form:

$$\frac{\partial}{\partial t}\left(\eta\left(\frac{\bar{u}^2}{2}+\frac{e}{2}+\frac{\eta+2h}{2}\right)\right)+\frac{\partial}{\partial x}\left(\eta\bar{u}\left(\frac{\bar{u}^2}{2}+e+\frac{\eta+2h}{2}\right)+\frac{\eta^2}{2}\bar{u}\right)$$

$$=M\left(\frac{u^2}{2}\Big|_{z=h}+h\right)+p\big|_{z=h}(h_t+M).$$

Remark 1 The term M which is responsible for the mixing, should be specified. In applications, we take it in the form

$$M=\sigma\sqrt{e},\quad \sigma=\text{const}, \tag{17}$$

where σ is the shear coefficient (the ratio between the averaged over the fluid depth shear stress and the turbulent kinetic energy):

$$-\frac{1}{h}\int_h^{h+\eta}\tilde{u}\tilde{w}dz=\sigma e. \tag{18}$$

Here 'tilde' means the velocity fluctuations. In a vertically sheared flow the sign of σ coincides with the sign of the vertical mean velocity gradient. The value of σ is about 0.15 ((35), (4)). The justification of (17) can be done in the following way. We denote the classical Reynolds averaging of the dimensionless Euler equations (with $\varepsilon=1$) by angle brackets $\langle ...\rangle$, with a classical representation for any f in the form $f=\langle f\rangle+\tilde{f}$, where $\langle\tilde{f}\rangle=0$. The corresponding dimensionless Reynolds equations are

$$\langle u\rangle_x+\langle w\rangle_z=0,\quad \langle u\rangle_t+\left(\langle u\rangle^2+\langle\tilde{u}^2\rangle+\langle p\rangle\right)_x+\left(\langle u\rangle\langle w\rangle+\langle\tilde{u}\tilde{w}\rangle\right)_z=0,$$

$$\langle w\rangle_t+\left(\langle u\rangle\langle w\rangle+\langle\tilde{u}\tilde{w}\rangle\right)_x+\left(\langle w\rangle^2+\langle\tilde{w}^2\rangle+\langle p\rangle\right)_z=-1,$$

$$\langle E\rangle_t+\left(\langle u\rangle\langle E\rangle+\langle\tilde{u}\tilde{E}\rangle+\langle p\rangle\langle u\rangle+\langle\tilde{p}\tilde{u}\rangle\right)_x$$

$$+\left(\langle w\rangle\langle E\rangle+\langle\tilde{w}\tilde{E}\rangle+\langle p\rangle\langle w\rangle+\langle\tilde{p}\tilde{w}\rangle\right)_z=-\langle w\rangle. \tag{19}$$

Here we denoted

$$E=\frac{u^2+w^2}{2},\quad \langle E\rangle=\frac{\langle u\rangle^2+\langle w\rangle^2}{2}+\frac{e}{2},\quad e=\langle\tilde{u}^2\rangle+\langle\tilde{w}^2\rangle,$$

$$\tilde{E}=\langle u\rangle\tilde{u}+\langle w\rangle\tilde{w}+\frac{\tilde{u}^2+\tilde{w}^2}{2}-\frac{e}{2}.$$

Consider now particular solutions of (19) where all the variables depend only on (t,z), and the vertical average velocity $\langle w\rangle$ is zero. Also, we will assume

that the third order correlations and the correlation $\langle \tilde{p}\tilde{w}\rangle$ are negligible. Such a solution is suitable for the description of the mixing layer. Equations (19) imply

$$\langle u\rangle_t + (\langle \tilde{u}\tilde{w}\rangle)_z = 0, \quad \left(\frac{\langle u\rangle^2}{2} + \frac{e}{2}\right)_t + \left(\langle \tilde{u}\tilde{w}\rangle\langle u\rangle\right)_z = 0. \tag{20}$$

System (20) simplifying (19) with the closure $-\langle \tilde{u}\tilde{w}\rangle = \sigma e$ is hyperbolic, with the characteristic slopes $\pm\sigma\sqrt{2e}$. The mixing front between the turbulent layer and the potential layer can be seen as a shock separating the two regions. Applying the Rankine–Hugoniot relations coming from (20) we obtain

$$D[\langle u\rangle] + \sigma\,[e] = 0, \quad D\left[\frac{\langle u\rangle^2}{2} + \frac{e}{2}\right] + \sigma[e\langle u\rangle] = 0.$$

Here the square brackets mean the jump of variables. Let u^-, e^-, and u^+, $e^+ = 0$ be the values of unknowns in the turbulent and potential region, respectively, with $u^- > u^+$. Then we have :

$$e^- = (u^- - u^+)^2, \quad D = -\sigma\frac{(u^- - u^+)^2}{u^- - u^+} = -\sigma\sqrt{e^-}.$$

This is exactly the empirical relation (17) defining M. The sign 'minus' corresponds to the fact that η is growing at the same time as z is decreasing. Such a shock is stable in the sense of Lax (the characteristics overlap at the shock). A detailed discussion can also be found in Liapidevskii & Teshukov (2000) (18).

Remark 2 The turbulent energy dissipation toward smaller scales (smaller then the scale of large vortexes defined by η) should also be added. The most simple empirical expression for the energy dissipation rate d can be taken in the form ((35)):

$$d = \sigma\frac{\kappa}{2}e^{3/2} = M\frac{\kappa}{2}e. \tag{21}$$

Here the coefficient $\kappa/2$ is of order one, the factor $1/2$ is added for convenience. The shear coefficient σ has an effect on the length of surface waves, while the dissipation coefficient κ is responsible for the turbulent layer thickness development.

Remark 3 The model derived is a 'dispersive generalization' a two-layer hydrostatic model with shear (turbulence) effects in the upper layer proposed in Liapidevskii & Chesnokov (2014)(20). The dispersive effects are more important in the lower layer while the shear (turbulence) effects are more important in the upper layer. The model is more general than that proposed in Richard & Gavrilyuk (2015) (27) where a dispersive model for shear flows was derived. In that paper, a small thickness upper shear layer was also introduced, but its dynamical development was assumed to be negligible. The approach by Antuono & Brocchini (2013) (1) where Reynolds averaging and depth averaging were combined for the derivation of an integro-differential system for wave propagation has some similarity with our approach because it also enables a better modelling of the turbulent energy evolution. A close model combining both

shear and dispersive effects, but containing also third order correllations of the velocity, was recently proposed by Castro and Lannes (2014)(7). It supposes a regularity of the velocity field in the vertical direction, while in our model the velocity field is singular (two layer system).

2.3 Final two-layer system

The final dimensionless system can be written as

$$\frac{\partial \eta}{\partial t} + \frac{\partial \eta \bar{u}}{\partial x} = M, \tag{22}$$

$$\frac{\partial}{\partial t}(\eta \bar{u}) + \frac{\partial}{\partial x}\left(\eta \bar{u}^2 + \eta e + \frac{\eta^2}{2}\right) = MU - \eta h_x, \tag{23}$$

$$\frac{\partial}{\partial t}\left(\eta\left(\frac{\bar{u}^2}{2} + \frac{e}{2} + \frac{\eta + 2h}{2}\right)\right) + \frac{\partial}{\partial x}\left(\eta\bar{u}\left(\frac{\bar{u}^2}{2} + \frac{e}{2} + \frac{\eta + 2h}{2}\right) + \left(\eta e + \frac{\eta^2}{2}\right)\bar{u}\right) \tag{24}$$
$$= M\left(\frac{U^2}{2} + h\right) + \eta(h_t + M) - d,$$

$$\frac{\partial h}{\partial t} + \frac{\partial}{\partial x}(hU) = -M, \tag{25}$$

$$\frac{\partial}{\partial t}(hU) + \frac{\partial}{\partial x}\left(hU^2 + \int_0^h p\, dz\right) = \eta h_x - MU, \tag{26}$$

$$\frac{\partial}{\partial t}\left(h\left(\frac{U^2}{2} + \varepsilon^2\frac{U_x^2}{6}h^2 + \frac{h}{2}\right)\right) + \frac{\partial}{\partial x}\left(hU\left(\frac{U^2}{2} + \varepsilon^2\frac{U_x^2}{6}h^2 + \frac{h}{2}\right) + U\int_0^h p\, dz\right) \tag{27}$$
$$= -\eta(h_t + M) - M\left(\frac{U^2}{2} + \varepsilon^2\frac{U_x^2 h^2}{2} + h\right),$$

with

$$\int_0^h p\, dz = \eta h + \frac{h^2}{2} - \varepsilon^2\frac{h^3}{3}(U_{xt} + UU_{xx} - U_x^2), \quad M = \sigma\sqrt{e}, \quad d = M\frac{\kappa}{2}e. \tag{28}$$

The system (22)- (28) admits the total momentum conservation law:

$$\frac{\partial}{\partial t}(\eta\bar{u} + hU) + \frac{\partial}{\partial x}\left(\eta\bar{u}^2 + \eta e + \frac{\eta^2}{2} + hU^2 + \int_0^h p\, dz\right) = 0,$$

and the total energy balance equation :

$$\frac{\partial}{\partial t}\left(\eta\left(\frac{\bar{u}^2}{2} + \frac{e}{2} + \frac{\eta + 2h}{2}\right) + h\left(\frac{U^2}{2} + \varepsilon^2\frac{U_x^2}{6}h^2 + \frac{h}{2}\right)\right)$$

$$+\frac{\partial}{\partial x}\left(\eta\bar{u}\left(\frac{\bar{u}^2}{2} + \frac{e}{2} + \frac{\eta + 2h}{2}\right) + \left(\eta e + \frac{\eta^2}{2}\right)\bar{u} + hU\left(\frac{U^2}{2} + \varepsilon^2\frac{U_x^2}{6}h^2 + \frac{h}{2}\right) + U\int_0^h p\, dz\right)$$

$$= -M\varepsilon^2 \frac{U_x^2 h^2}{2} - d.$$

Since $M > 0$ (the thickness of the upper layer is increasing because of the developing the turbulent layer) and $d > 0$, the total energy is decreasing. The energy equation for the lower layer (27) is not independent, it is a consequence of (25) and (26).

2.4 An equivalent form of the momentum equation for the lower layer

The flux in the momentum equation (26) for the lower layer contains the higher order derivatives of the velocity U. It appears, that for numerical purposes the following new variable

$$K = U - \frac{\varepsilon^2}{3h}\big(h^3 U_x\big)_x$$

is more convenient for the model formulation. The variable K is nothing but the tangential velocity along the free surface (cf. Gavrilyuk & Teshukov, 2001, Bardos & Lannes, 2012, Gavrilyuk, Kalisch & Khorsand, 2015). For this, we replace the momentum equation by an equivalent equation (see Appendix B for the proof) :

$$K_t + \left(KU + h + \eta - \frac{U^2}{2} - \frac{\varepsilon^2}{2}U_x^2 h^2 - \varepsilon^2 h M U_x\right)_x = M\left(\frac{K-U}{h} + \varepsilon^2 h_x U_x\right).$$

In the case where the mixing is absent ($M = 0$), this equation is reduced to the conservative one :

$$K_t + \left(KU + h + \eta - \frac{U^2}{2} - \frac{\varepsilon^2}{2}U_x^2 h^2\right)_x = 0.$$

2.5 Production of the turbulent energy

An evolution equation for the turbulent energy e in the upper layer can also be obtained. Consider the subsystem for the upper layer (22) – (24). Using the equation of the mass (22) and the momentum (23) one can obtain from (24) :

$$\frac{\eta}{2}\frac{\bar{D}e}{Dt} + e\left(M - \frac{\bar{D}\eta}{Dt}\right) = M\left(\frac{(U-\bar{u})^2}{2} - \frac{e}{2}\right) - d, \quad \frac{\bar{D}}{Dt} = \frac{\partial}{\partial t} + \bar{u}\frac{\partial}{\partial x}.$$

It is equivalent to :

$$\frac{\eta}{2}\frac{\bar{D}e}{Dt} - e\frac{\bar{D}\eta}{Dt} = M\left(\frac{(U-\bar{u})^2}{2} - \frac{3}{2}e\right) - d.$$

It implies :

$$\frac{\bar{D}}{Dt}\left(\frac{e}{\eta^2}\right) = \frac{M}{\eta^3}\Big((U-\bar{u})^2 - (3+\kappa)e\Big).$$

For numerics, a conservative equation for q will be used. Replacing e by q^2 and using the equation for η one can derive a conservative equation for q

$$\frac{\partial q}{\partial t} + \frac{\partial}{\partial x}(q\bar{u}) = \frac{\sigma}{2\eta}\Big((U-\bar{u})^2 - (1+\kappa)q^2\Big).$$

2.6 Flow over topography

The derivation of the governing equations for the flow over topography is analogous. However, such a derivation can considerably be simplified under the following assumption on the bottom variation. Let $z = b(x)$ be the bottom variation. Then the most simple approach is to add in the right-hand side of the dimension momentum equation for the upper layer the term $-g\eta b_x$, and in the equation for K the term $-gb_x$. It corresponds to the dimensionless scaling $b(x) \to b(\varepsilon^\alpha x)$ with $\alpha > 0$, allowing us to neglect the second derivatives and the squared first derivatives of b. Only the first space derivative of b will be kept, as it is the case of non-dispersive shallow water equations. Such an approach was used, for example, in Serre (1953)(29) and Liapidevskii & Gavrilova (2008) (19).

3 Stationary solutions for a flat bottom

The governing equations (22)- (28) are Galilean invariant. The study of the travelling wave solution is thus equivalent to the study of the stationary solutions. We denote by 'prime' the derivative with respect to x. Continuous stationary solutions written in dimension form satisfy the equations:

$$(\eta\bar{u})' = \sigma q, \quad \left(\eta\bar{u}^2 + \eta q^2 + \frac{g\eta^2}{2}\right)' = \sigma q U - g\eta h', \tag{29}$$

$$\eta\bar{u}q' - q\bar{u}\eta' = \frac{\sigma}{2}\Big((U-\bar{u})^2 - (3+\kappa)q^2\Big),$$

$$(hU)' = -\sigma q, \quad \Big(hU^2 + P\Big)' = g\eta h' - \sigma q U,$$

with

$$P = \frac{gh^2}{2} + gh\eta - \frac{h^3}{3}\left(UU'' - U'^2\right).$$

The normal form of (29) is

$$h' = -\frac{\sigma q + hW}{U}, \tag{30}$$

$$\eta' = \frac{1}{\Delta}\left(\sigma q\left(2\bar{u} - U + \frac{1}{\bar{u}}\Big((U-\bar{u})^2 - (3+\kappa)q^2\Big)\right) + g\eta h'\right),$$

$$\bar{u}' = \frac{\sigma q - \bar{u}\eta'}{\eta}, \quad U' = W, \quad W' = Z,$$

$$Z' = \frac{3}{Uh^2}\Big(UW + g(h'+\eta') + \frac{h^2}{3}WZ - h(UZ - W^2)h'\Big),$$
$$q' = \frac{1}{2\eta\bar{u}}\Big(\sigma\Big((U-\bar{u})^2 - (3+\kappa)q^2\Big) + 2q\bar{u}\eta'\Big).$$

Here

$$\Delta = \bar{u}^2 - g\eta - 3q^2. \tag{31}$$

The 'true' normal form is obtained by replacing also the derivatives η' and h' by the corresponding algebraic relations. To avoid cumbersome expressions, we will present only a reduced form (30). The variables describing the lower dispersive layer (U and h) are always continuous in the flow. However, the variables describing the upper turbulent layer may be discontinuous when the supercritical-subcritical transition occurs. If the stationary solution is discontinuous, the following Rankine–Hugoniot relations for the upper layer are satisfied :

$$[\eta\bar{u}] = 0, \quad \left[\eta\bar{u}^2 + \eta e + \frac{1}{2}g\eta^2\right] = 0, \quad \left[\frac{\bar{u}^2}{2} + \frac{3}{2}e + g\eta\right] = 0. \tag{32}$$

Here the square brackets mean the jump of the corresponding quantities. Relations (32) are usual conservation of mass, momentum and energy in the upper layer. Also, the momentum equation for the lower layer implies :

$$\left[g\eta h - \frac{h^3}{3}UU''\right] = 0. \tag{33}$$

Here we used the continuity of h, U and U' at the shock. Formula (33) gives us the jump of the second derivative U'' at the shock. The jump is not zero because the jump of η is non-vanishing.

We are looking for stationary solutions of (30) having supercritical constant potential flow as $x \to -\infty$:

$$(\bar{u}, U) \to (U_0, U_0),\ U_0 > 0 \quad (\eta, h) \to (0, H_0), \quad e \to 0, \quad F = U_0/\sqrt{gH_0} > 1. \tag{34}$$

The flow is potential at negative infinity, so the upper turbulent layer and the corresponding turbulent energy are vanishing. To construct such a solution, it is necessary first to understand the asymptotic behaviour of the supercritical solution at negative infinity. Linearizing the equations for the total mass and the equation for the momentum of the lower layer we obtain (the perturbations are denoted by the same letters)

$$H_0U' + U_0(h' + \eta') = 0,$$
$$U_0u' + g(h' + \eta') - \frac{H_0^2}{3}U_0U'' = 0.$$

Eliminating $h' + \eta'$ we get the equation for U

$$\left(1 - \frac{1}{F^2}\right)U' - \frac{H_0^2}{3}U''' = 0.$$

It implies that as $x \to -\infty$ the solution in the lower layer behaves asymptotically as the solution of the Green–Naghdi equations:

$$U \approx \exp\left(\lambda \frac{x}{H_0}\right), \quad \lambda = \sqrt{3\left(1 - \frac{1}{F^2}\right)}.$$

Perturbations (nonlinear) for the upper layer variables satisfy the equations:

$$U_0 \eta' = \sigma q, \quad U_0 \bar{u}' - \frac{g H_0}{U_0} U' = \sigma \frac{q(U - \bar{u})}{\eta}, \quad U_0 q' = \sigma \frac{(U - \bar{u})^2 - (1 + \kappa) q^2}{2\eta}.$$

Looking for the solutions in the form

$$U = \hat{U} \exp\left(\lambda \frac{x}{H_0}\right), \quad \eta = \hat{\eta} \exp\left(\lambda \frac{x}{H_0}\right), \quad \bar{u} = \hat{\bar{u}} \exp\left(\lambda \frac{x}{H_0}\right), \quad q = \hat{q} \exp\left(\lambda \frac{x}{H_0}\right)$$

we obtain the following expressions for unknown amplitudes :

$$\hat{\bar{u}} = \frac{\hat{U}}{2}\left(1 + \frac{1}{F^2}\right), \quad \hat{q} = -\frac{\hat{U}}{2\sqrt{3 + \kappa}}\left(1 - \frac{1}{F^2}\right), \quad \hat{\eta} = \frac{\sigma H_0}{\lambda U_0}\hat{q}, \quad \hat{h} = -\frac{H_0}{U_0}\hat{U} - \hat{\eta}. \tag{35}$$

The sign in the expression of $\hat{q}$ is minus because $\hat{U} < 0$. Also, it is interesting to note that in this case

$$\hat{U} - \hat{\bar{u}} = \frac{\hat{U}}{2}\left(1 - \frac{1}{F^2}\right) < 0$$

because $F^2 > 1$. It means that at the beginning of mixing the velocity in the upper layer is larger than the velocity in the lower layer. Asymptotic expressions (35) were used when the conditions at the negative infinity are imposed in the numerical treatment of the stationary system. We used MATHEMATICA 10.1 edition to solve the first order system (30).

3.1 The structure of stationary solutions

The mixing process is dissipative, so the stationary solution is rather an undular bore, and not a sequence of solitary (or periodic) waves. The upper layer is developing quite slowly if the flow is supercritical everywhere (the determinant (31) is positive). A typical flow picture is shown in Figure 2.

There exists a critical Froude number $F_\star$ such that the flow becomes critical (the determinant (31) vanishes) at the top of the leading wave. This value can easily be numerically determined. For example, $F_\star \approx 1.338$ for $\kappa = 0$.

One can also find another critical value $F_{\star\star}$ for which the determinant vanishes at the top of the second wave. For example, $F_{\star\star} \approx 1.283$ for $\kappa = 0$. A sequence of the corresponding critical values can thus be constructed. The smaller the Froude number is (but always larger then one), the larger the domain, where the solution is supercritical, is. The critical Froude numbers increase with increasing κ. For example, for $\kappa = 3$, one has $F_\star \approx 1.3832$, and $F_{\star\star} \approx 1.3201$.

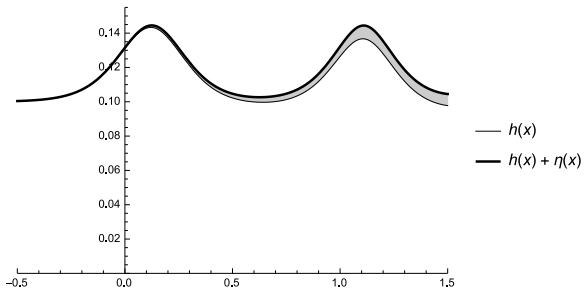

Figure 2: A typical supercritical stationary flow for the Froude number $F = 1.2$ is shown. The lower boundary separates potential and turbulent layers. The mixing region of thickness η is gradually increasing. The parameters are as follows: $H_0 = 0.1\ m$, $U_0 = 1.19\ m/s$, $g = 9.81\ m/s^2$, $\sigma = 0.15$, $\kappa = 0$.

When the supercritical–subcritical transition happens, i.e. the determinant (31) changes the sign from positive to negative, the solution may contain a jump of the variables of the upper turbulent layer. The thickness of the upper layer in the subcritical local zone will rapidly increase in downflow because of the mixing process. The pressure distribution is approaching to the hydrostatical because the turbulent layer will expand. The transition can occur not necessarily at the leading wave, but, for example, at the second wave.

Now we will show how to construct another solution containing a jump riding down the forward slope of the leading wave even for $F < F_\star$. The construction of such a solution can be done as follows. Take any Froude number $F < F_\star$. We put the jump at a point $x = x_0$ which should be properly chosen. For given values $\eta_0 = \eta(x_0), \bar{u}_0 = \bar{u}(x_0), q_0 = q(x_0)$ one can use the Rankine–Hugoniot relations (32):

$$\eta\bar{u} = \eta_0\bar{u}_0 = Q, \quad \eta\bar{u}^2+\eta q^2+\frac{g}{2}\eta^2 = \eta_0\bar{u}_0^2+\eta_0 q_0^2+\frac{g}{2}\eta_0^2, \quad \frac{\bar{u}^2}{2}+\frac{3}{2}q^2+g\eta = \frac{\bar{u}_0^2}{2}+\frac{3}{2}q_0^2+g\eta_0.$$

Eliminating the velocities, one can obtain a quadratic equation for the layer thickness after the jump

$$\frac{g}{2}\eta_0^2\eta^2 - \eta\left(Q^2 + 3\eta_0\left(\frac{1}{2}g\eta_0^2 + \eta_0 q_0^2\right)\right) + 2\eta_0 Q^2 = 0.$$

The equation has two positive roots. Only one of them (the minimal one) having the property $\eta < 2\eta_0$ must be chosen (see the discussion in Richard & Gavrilyuk, 2012). Since the value of η_0 is almost negligible, the jump of η is almost invisible. However, the corresponding turbulent energy considerably increases. The flow in the turbulent region becomes subcritical. The thickness of the turbulent layer is increasing, the flow in this layer decelerates and the determinant (31) in the equation for η vanishes at some point $x = x_1$. If at the same point the numerator vanishes, the solution can be extended again to the

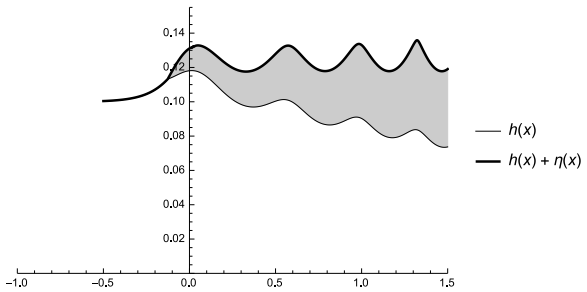

Figure 3: A new supercritical–subcritical stationary solution for the Froude number $F = 1.2$ is shown. The subcritical turbulent region rapidly increases after the jump. The flow continuously passes to the supecritical regime. The flow parameters are as follows: $H_0 = 0.1\ m$, $U_0 = 1.19\ m/s$, $g = 9.81\ m/s^2$, $\sigma = 0.15$, $\kappa = 0$. The supercritical–subcritical transition is at the point $x_0 \approx -0.124$, the subcritical–supercritical transition is at the point $x_1 \approx 0.025$.

supercritical region for $x > x_1$. The value of $x = x_0$ can always be chosen, and thus a new solution containing a local subcritical zone between x_0 and x_1 can be constructed. Such a new solution is shown in Figure 3 for the Froude number $F = 1.2$. The local zone where the solution is subcritical, can be associated to the wave breaking.

These two solutions have completely different properties. The first one, without the jump, has long modulations and quite narrow mixture region (Figure 2). The second one, with a jump, has shorter modulations at the same space interval, smaller amplitude, and thicker mixture zone (see Figure 3). The same boundary conditions at the negative infinity can thus produce completely different stationary solutions. Such a non-uniqueness of the stationary solutions is often associated with the hysteresis phenomenon, where one or another solution can appear through non-stationary scenarios.

The model also contains a criterion of wave breaking which is characterized by the Froude number between 1.3 and 1.4 depending on the energy dissipation parameter κ. An interesting feature of this model is a possibility of existence of a local subcritical zone $[x_0, x_1]$ which can be associated with the wave breaking. The non-stationary wave breaking will be studied in the next sections.

4 Applications to non-stationary problems

4.1 Numerical method

For numerical treatment the following dimension form of the governing equations is used :

$$\begin{aligned}
&\frac{\partial \eta}{\partial t} + \frac{\partial}{\partial x}(\eta\bar{u}) = \sigma q, \quad \frac{\partial}{\partial t}(h+\eta) + \frac{\partial}{\partial x}(hU + \eta\bar{u}) = 0,\\
&\frac{\partial}{\partial t}(\eta\bar{u}) + \frac{\partial}{\partial x}\Big(\big(\bar{u}^2 + q^2\big)\eta + \frac{g\eta^2}{2}\Big) = \sigma q U + \alpha_1,\\
&\frac{\partial q}{\partial t} + \frac{\partial}{\partial x}(q\bar{u}) = \frac{\sigma}{2\eta}\Big((U-\bar{u})^2 - (1+\kappa)q^2\Big),\\
&\frac{\partial K}{\partial t} + \frac{\partial}{\partial x}\Big(KU + g(h+\eta) - \frac{U^2}{2} + \alpha_2\Big) = \sigma q\Big(\frac{K-U}{h} + \alpha_3\Big) - g b_x,
\end{aligned} \tag{36}$$

where

$$\alpha_1 = -g\eta(h+b)_x, \quad \alpha_2 = -\frac{U_x^2 h^2}{2} - h\sigma q U_x, \quad \alpha_3 = h_x U_x, \tag{37}$$

and the velocity U is determined by the equation

$$K = U - \frac{1}{3h}\big(h^3 U_x\big)_x. \tag{38}$$

For a given K, (38) is an ordinary differential equation for U. The function $z = b(x)$ defines the bottom variation; σ and κ are constants. The preceding system (36) can be written in conservative form :

$$\frac{\partial \mathbf{u}}{\partial t} + \frac{\partial \mathbf{f}}{\partial x} = \mathbf{g}, \tag{39}$$

where

$$\mathbf{u} = \big(\eta,\, h+\eta,\, \eta\bar{u},\, q,\, K\big)^{\mathrm{T}},$$

$$\mathbf{f} = \Big(\eta\bar{u},\, hU + \eta\bar{u},\, \big(\bar{u}^2+q^2\big)\eta + \frac{g\eta^2}{2}, q\bar{u}, KU + g(h+\eta) - \frac{U^2}{2} + \alpha_1\Big)^{\mathrm{T}},$$

$$\mathbf{g} = \Big(\sigma q,\, 0,\, \sigma q U + \alpha_1,\, \frac{\sigma}{2\eta}\Big((U-\bar{u})^2 - (1+\kappa)q^2\Big),\, \sigma q\Big(\frac{K-U}{h} + \alpha_3\Big) - g b_x\Big)^{\mathrm{T}}.$$

Following Le Metayer *et al.* (2010) (17) we divide the numerical resolution of system (36) into three successive steps:

1) the numerical approximations of the terms α_i, $i = 1, 2, 3$, containing spatial derivatives (see relations (37));

2) the time evolution of the conservative variables $\mathbf{u}$ using the method based on modification of Godunov's scheme;

3) the resolution of an ordinary differential equation (38) to obtain the values of velocity U from variables h and K.

To solve differential balance laws (39) numerically we implement here the Nessyahu & Tadmor (1990)(24) second-order central scheme (see also Russo (2005) (28)) :

$$\begin{aligned}
&\mathbf{u}_j^{n+1/2} = \mathbf{u}_j^n - \Lambda \mathbf{f}_j'/2 + \mathbf{g}(\mathbf{u}_j^n)\Delta t/2, \qquad (\Lambda = \Delta t/\Delta x) \\
&\mathbf{u}_{j+1/2}^{n+1} = (\mathbf{u}_j^n + \mathbf{u}_{j+1}^n)/2 + (\mathbf{u}_j' - \mathbf{u}_{j+1}')/8 - \Lambda\big(\mathbf{f}(\mathbf{u}_{j+1}^{n+1/2}) - \mathbf{f}(\mathbf{u}_j^{n+1/2})\big) \\
&\qquad\qquad + \big(\mathbf{g}(\mathbf{u}_j^n + \mathbf{g}(\mathbf{u}_{j+1}^n)\big)\Delta t/2.
\end{aligned} \tag{40}$$

Here $\mathbf{u}_j^n = \mathbf{u}(t^n, x_j)$, Δx is the spatial grid spacing, and Δt is the time-step satisfying the Courant condition, defined by the velocity of characteristics of the dispersionless part of the model. The computational domain on the x axis is divided into N cells, the cell centres are denoted by x_j. Values $\mathbf{u}_j'/\Delta x$ and $\mathbf{f}_j'/\Delta x$ are approximations of the first-order derivatives with respect to x, calculated according to the 'MinMod' procedure. At $t = 0$ the initial data $\mathbf{u}_j^0$ are specified. The boundary conditions $\mathbf{u}_{1-k}^n$ and $\mathbf{u}_{N+k}^n$ $(k = 1, 2)$ are also should be prescribed. Since the state $\mathbf{u}_j^n$ is known using formulae (40) one can obtain the conservative variable $\mathbf{u}$ at time t^{n+1}. Scheme (40) does not require exact or approximate solution of the Riemann problem that is very convenient in our case, since system (36) includes five equations. It should be noted that other schemes (in particular, on non-staggered grids) based on the local Lax–Friedrichs flux are also appropriate here.

The numerical estimation of the first order derivatives of any function φ at $x = x_j$ is given by the following relation

$$\left(\frac{\partial \varphi}{\partial x}\right)_j = \frac{\varphi_{j+1/2} - \varphi_{j-1/2}}{\Delta x}, \quad \varphi_{j\pm1/2} = \frac{\varphi_{j\pm1} + \varphi_j}{2}\,. \tag{41}$$

This discretization is used to determine the terms α_i in (37). As a result we obtain the flux $\mathbf{f}_j^n$ at time t^n.

The last ingredient concerns the determination of the velocity U_j at the next time step when the vector of conservative variables $\mathbf{u}_j^{n+1}$ is known. Applying finite difference discretization (41) one can rewrite equation (38) in the following form

$$a_{j-1}U_{j-1} - c_jU_j + b_jU_{j+1} = -f_j, \quad (j = 1, ..., N) \tag{42}$$

where

$$a_i = h_{j-1/2}^3, \quad b_j = h_{j+1/2}^3, \quad c_j = a_j + b_j + 3\Delta x^2 h_j, \quad f_j = 3\Delta x^2 h_j K_j.$$

All the variables in the preceding relation are those at time t^{n+1}. As a consequence, the variables h_j and K_j are known and come from the time evolution of conservative variables with the help of the numerical scheme presented above. The only unknowns are the terms U_j at each node. Relations represent a tridiagonal system of linear equations that can be solved by a direct (Gauss) method. We apply here a simplified form of Gaussian elimination which is known as the Thomas algorithm.

The next section is devoted to numerical results obtained with the present method for different applications.

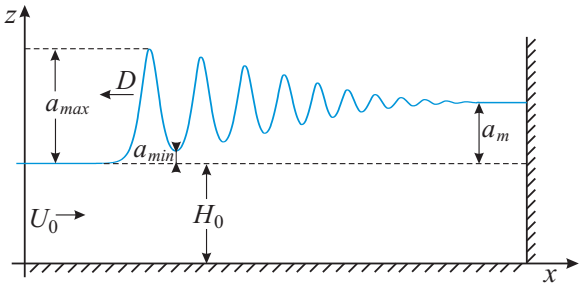

Figure 4: Definition sketch for the Favre waves.

4.2 'Water hammer problem with a free surface' (Favre waves)

Pioneering experimental works concerning the development of undular bores were performed by Favre (1935), who studied their formation in long open channels due to a rapid opening or closing of a gate. Similar experiments with a detailed investigation of the formation of surge waves in open channels were performed by Treske (1994) (36) and by Soares-Frazão & Zech (2002)(30). Analytical approach to the study of undular bores was developed in El *et al.* (2005, 2006) within a framework of the Serre–Su–Gardner–Green–Naghdi equations (Serre, 1953, Su & Gardner, 1969, Green & Naghdi, 1976). This problem was studied numerically in Soares-Frazão & Guinot (2008)(31) and in Tissier *et al.* (2011)(34). Laboratory experiments (Treske (1994)(36) and Chanson (2009)(8)) showed that the wave Froude number F which is defined as

$$F = \frac{U_0 - D}{\sqrt{gH_0}} \tag{43}$$

controls the bore shape. In supercritical regime ($F > 1$), undulations start developing at the bore front in the near-critical state ($F \approx 1$). However, when the Froude number is approximately between 1.3 and 1.4, the transition from the undular bore to the bore consisting of a steep front (breaking bore) occurs. Figure 4 shows a definition sketch for the Favre waves in the undular regime. Constants U_0 and H_0 are the upstream flow velocity and depth. In the following D denotes the propagation speed of the wave front; a_m represents the jump height; a_{max} and a_{min} are the maximum and minimum amplitude of the first wave. Below we present some results related to the numerical modelling of Favre waves on the base of equations (36)–(38) in the domain of the Froude number between 1 and 1.3 corresponding to the domain of existence of the undular bore. We also demonstrate transition from undular to purely breaking bores with increasing of the Froude number, and, in particular, compare numerical results for the first wave amplitude with experimental data (Treske (1994)(36)).

We perform calculations in dimensionless variables in the domain $x \in [0, 100]$ for $N = 1000$. We take here $g = 1$, $\sigma = 0.15$ and $\kappa = 3$. To start calculations

we specify unknown variables $\mathbf{u}$ in the node points $x = x_j$ at $t = 0$ as follows $\eta = 0.01$, $h + \eta = 1$, $\bar{u} = K = U_0$, and $q = 0$. On the left boundary we assume that $\mathbf{u}^n_{1-k} = \mathbf{u}^n_1$. These conditions allow us to calculate until the perturbations reach the boundary of the computational domain. To satisfy impermeability condition ($\bar{u} = U = 0$) on the right wall $x = 100$ we use the reflecting boundary conditions: $\mathbf{u}^n_{N+k} = \mathbf{u}^n_{N-k}$ except of variables $\eta\bar{u}$ and K that are treated as $(\eta\bar{u})^n_{N+k} = -(\eta\bar{u})^n_{N-k}$ and $K^n_{N+k} = -K^n_{N-k}$.

It should be noted that instead of the upstream velocity U_0 it is more convenient to prescribe the upstream Froude number F. A simple relation between them can be obtained. Indeed, according to conservation of mass and momentum we have the following relations (in dimension variables) :

$$\begin{aligned} &(U_0 - D)H_0 = (U_1 - D)H_1, \\ &(U_0 - D)^2 H_0 + \frac{gH_0^2}{2} = (U_1 - D)^2 H_1 + \frac{gH_1^2}{2}, \end{aligned} \tag{44}$$

where U_0 and U_1 the upstream and downstream velocities, respectively, and H_0, $H_1 = H_0 + a_m$ the corresponding water depths. In our case $U_1 = 0$. The Bélanger formula

$$\frac{H_1}{H_0} = \frac{\sqrt{1 + 8F^2} - 1}{2} \tag{45}$$

is the consequence of (43) and (44). Taking into account (45) one can express U_0 from (44) in term of the Froude number:

$$U_0 = U_1 + \sqrt{gH_0}\left(F - \frac{1 + \sqrt{1 + 8F^2}}{4F}\right). \tag{46}$$

Figure 5 shows the results of computations at dimensionless time instant $t_* = 90$ for $F = 1.28$ (undular bore) and $F = 1.40$ (breaking bore) that correspond to the following upstream velocities : $U_0 = 0.3511$ and $U_0 = 0.4921$. Thus, the proposed model (36)–(38) allows one to describe both undular and breaking bores without any 'switching' criteria. In both cases the surface turbulent layer is formed and shear velocity q is generated. The thickness of the layer grows with increasing of the jump amplitude a_m (or the Froude number F). Also, it is interesting to note that the region of high turbulence (lower curve in the Figure corresponding to the scaled variable $q^* = q/U_0$) is situated at the crests of the waves (Figure 5*a* for undular bores), or immediately at the wave front (Figure 5*b* for breaking bores). In the last case the dispersion effects are clearly negligible and the hydrostatic approximation can be used. Such an intensive region of the turbulence can be associated with the roller appearance.

Further we compare the amplitudes of undular bores obtained by model (36)–(38) with experimental data of Treske (1994) (36) (p. 365, Fig. 21). In this case we perform calculations in the domain $x \in [0, 200]$ with $N = 4000$ for different Froude numbers from the interval $F \in [1.10, 1.30]$. For larger Froude numbers, the amplitude of the leading wave rapidly decreases and the transition to the breaking bore occurs. As in the previous case we choose $g = 1$, $H_0 = 1$,

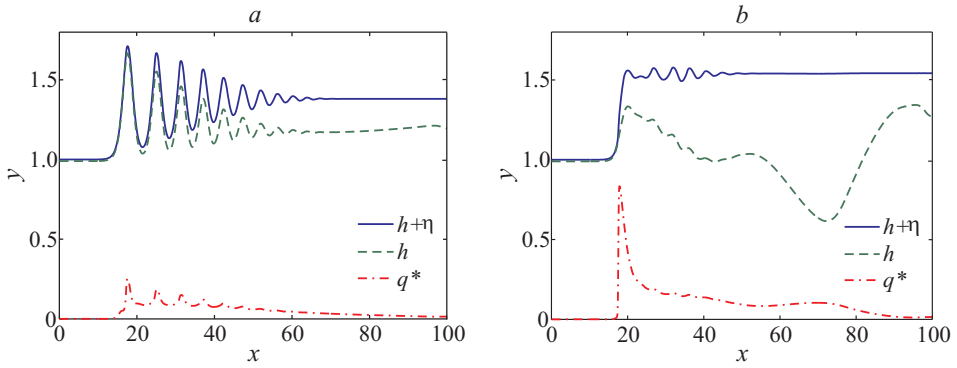

Figure 5: Favre waves: the free surface $h+\eta$, the thickness of the lower potential layer h, and the scaled shear velocity $q^* = q/U_0$ at $t_* = 90$, $t_* = t\sqrt{g/H_0}$ for $F = 1.28$ (a) and $F = 1.40$ (b). The parameters are as follows: $g = 1$, $\sigma = 0.15$, $\kappa = 3$.

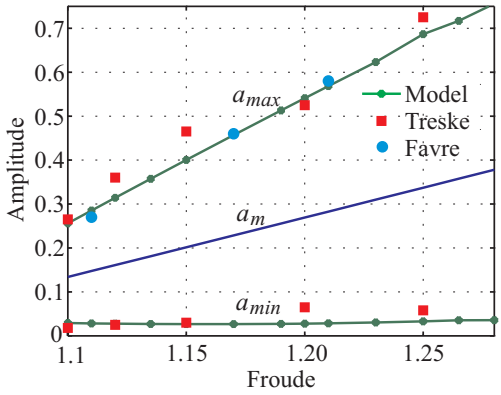

Figure 6: Amplitude of undulated bores for different Froude numbers.

$\sigma = 0.15$ and $\kappa = 3$. The maximum and minimum amplitude of the leading wave are taken at $t_* = 190$. Figure 6 shows that the results obtained by the model (36)–(38) are in good agreement with experimental data.

4.3 The shoaling and the breaking of the solitary wave

Here we consider the evolution of breaking solitary waves on a mild sloping beach and compare numerical results with experiments of Hsiao *et al.* (2008)(16). We perform calculations of the model (36)–(38) in the interval $x \in [0, 200]$. The bottom topography is specified as follows: $b(x) = 0$ for $x \in [0, 50]$; $b(x) = (x-50)/60$ for $x \in (50, 175)$; $b(x) = 25/12$ for $x \in [175, 200]$. To avoid modelling of the wave propagation over dry bottom (run-up) we introduce a shelf zone near the right boundary. On the both (left and right) walls we assume reflecting

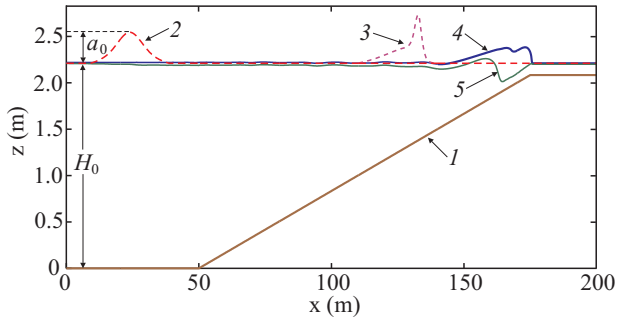

Figure 7: The evolution of solitary wave on a mild sloping beach: *1* — bottom topography; *2, 3*, and *4* — free surface at $t_* = 0$, 50, and 75, correspondingly; *5* — the boundary of lower potential layer at $t_* = 75$, where the dimensionless time t_* is given by $t_* = t\sqrt{g/H_0}$.

boundary conditions. Initial data represent a solitary wave having amplitude $a_0 = 0.3344\,m$ which propagates with the velocity $C_0 = \sqrt{g(a_0 + H_0)}$, where $H_0 = 2.2\,m$ is the undisturbed water depth, and $g = 9.8\,m/s^2$. These data correspond to trial 43 in experiments by Hsiao *et al.* (2008)(16). The initial thickness of the upper turbulent layer η_0 is equal to $0.01\,m$. The parameter values are as in the case of Favre waves : $\sigma = 0.15$, $\kappa = 3$. We take $N = 2000$ nodes for space resolution. Here we use dimensional variables.

Figure 7 shows the results of numerical calculations of the free surface at different time moments. As we can see from Figure 7, when the wave breaks the turbulent layer near free surface is formed (η is increasing).

The temporal evolution of the free surface displacements at different positions along the channel is shown in Figure 8. The numerical results were compared with the experimental data corresponding to trial 43 of the experiments by Hsiao *et al.* (2008)(16) (see Fig. 4 (a) on page 979). An excellent agreement with experimental data is observed everywhere except of region near the right boundary corresponding to $x = 172$ (the last graphic in Figure 8). This is due to the fact that we have introduced the shelf zone for $x > 175\,m$, while experimentally the wave continues to move on a sloping beach.

5 Conclusion

We constructed depth averaged governing equations for a two-layer long wave approximation of the homogeneous Euler equations with a free surface over a rigid bottom. The upper layer is turbulent and is described by system (22)–(24). The lower layer is almost potential and can be described by Serre– Su–Gardner–Green–Naghdi equations (25)–(28). The interface separating the two layers is considered as a discontinuity surface at which a turbulent mixing occurs. The constructed model reveals the main mechanism of the spilling breaker develop-

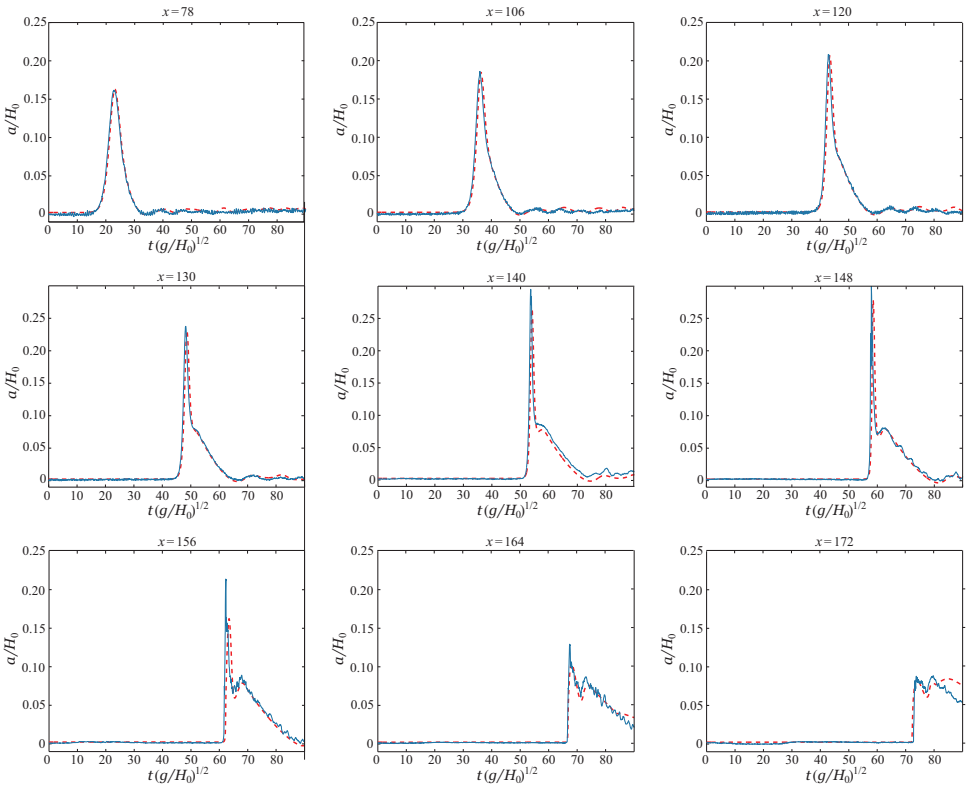

Figure 8: Time history of free surface displacement: solid curves — experimental data Hsiao *et al* (16), dashed curves — numerical results.

ment. For waves of moderate amplitude the upper thin layer is dynamically passive and the flow is principally governed by the dispersive model. However, for the waves of larger amplitude, the upper turbulent layer dynamics becomes crucial. The larger the wave amplitude, the greater the difference in the average flow velocities of layers is. It finally results in an intensive growing of the upper turbulent layer (spilling breaker formation).

In particular, the model predicts quite well the transition from undular bores to breaking bores. This point is very important. Indeed, the undular bore can be described by the dispersive Serre–Su–Gardner–Green– Naghdi model where a viscosity is added, but not the breaking bore. The breaking bore can be described by a hyperbolic model of the Saint–Venant type (see also a recent model proposed in Richard and Gavrilyuk (2012, 2013)), but not the undular bore. A combination of these simple model 'bricks' (dispersive and hyperbolic ones) allows us to obtain a natural transition between two types of bores. Also, a classical problem of the shoaling and the breaking of the solitary wave on a mild-slope beach is well predicted by the new model.

A future work will consist in the modelling of the air bubble entrainment by the breaking waves and a natural multi-dimensional extension of the model.

Acknowledgement The authors thank Shih - Chun Hsiao and Ting - Chieh Lin for providing the experimental data. The work was supported by the Russian Science Foundation (grant No. 15-11-20013). SG has been partially supported by the ANR project BoND (ANR-13-BS01-0009-01).

References

[1] Antuono, M. & Brocchini, M. 2013 Beyond Boussinesq-type equations: semi-integrated models for coastal dynamics. *Phys. Fluids* **25**, 016603.

[2] Bardos C. & Lannes, D. 2012 Mathematics for 2d interfaces. Singularities in Mechanics: Formation, Propagation and Microscopic Description (Panoramas et syntheses vol 38) (Paris: Société mathématique de France).

[3] Barros, R., Gavrilyuk S. & Teshukov, V. 2007 Dispersive nonlinear waves in two-layer flows with free surface. I. Model derivation and general properties. *Studies in Appl. Mathematics.* **119**, 191–211.

[4] Bradshaw, P., Ferriss, D. H. & Atwell, N. P. 1967 Calculation of boundary – layer development using the turbulent energy equation. *J. Fluid Mech.* **28**, 593–616.

[5] Brocchini, M. & Peregrine, D. H. 2001 The dynamics of strong turbulence at free surfaces. Part 1. Description *J. Fluid Mech.* **449**, 225–254.

[6] Brocchini, M. & Peregrine, D. H. 2001 The dynamics of strong turbulence at free surfaces. Part 2. Free-surface boundary conditions. *J. Fluid Mech.* **449**, 255–290.

[7] Castro, A., Lannes, D. 2014 Fully nonlinear long-wave models in the presence of vorticity. *J. Fluid Mech.* **759**, 642–675.

[8] Chanson, H. 2009 Current knowledge in hydraulic jumps and related phenomena. A survey of experimental results. *Europ. J. Mech. B/Fluids* **28** (2), 191–210.

[9] Duncan, J. H. 2001 Spilling Breakers. *Annu. Rev. Fluid Mech.* **33**, 519–547.

[10] El, G. A., Grimshaw, R. H. J. & Kamchatnov, A. M. 2005 Analytic model for a weakly dissipative shallow water undular bore. *Chaos* **15**, 037102.

[11] El, G. A., Grimshaw, R. H. J. & Smyth, N. F. 2006 Unsteady undular bores in fully non-linear shallow-water theory. *Phys. Fluids* **18**, 027104.

[12] Favre, H. 1935 Ondes de translation dans les canaux découverts. Dunod (Paris).

[13] Gavrilyuk, S. L. & Teshukov, V. M. 2002 Generalized vorticity for bubbly liquid and dispersive shallow water equations. *Continuum Mechanics and Thermodynamics* **13**, 365–382.

[14] Gavrilyuk, S., Kalisch, H. & Khorsand, Z. 2015 A kinematic conservation law in free surface flow. *Nonlinearity* **28** (6), 1805.

[15] Green, A. E. & Naghdi, P. M. 1976 A derivation of equations for wave propagation in water of variable depth. *J. Fluid Mech.* **78** 237–246.

[16] Hsiao, S.-C., Hsu, T.-W., Lin, T.-C. & Chang, Y.-H. 2008 On the evolution and run-up of breaking solitary waves on a mild sloping beach. *Coast. Eng.* **55**, 975–988.

[17] Le Metayer, O., Gavrilyuk, S. & Hank, S. 2010 A numerical scheme for the Green–Naghdi model. *J. Comput. Phys.* **229**, 2034–2045.

[18] Liapidevskii, V. Yu. & Teshukov, V. M. 2000 *Mathematical models of long wave propagation in non-homogeneous fluid.* Siberian Division of the Russian Academy of Sciences, Novosibirsk (in Russian).

[19] Liapidevskii, V. Yu. & Gavrilova, K. N. 2008 Dispersion and blockage effects in the flow over a sill. *J. Appl. Mech. Tech. Phys.* **49** (1), 34–45.

[20] Liapidevskii, V. Yu. & Chesnokov, A. A. 2014 Mixing layer under a free surface. *J. App. Mech. Tech. Phys.* **55** (2), 299–310.

[21] Longuet-Higgins, M. S. & Turner, J. S. 1974 An 'entraining plume' model of a spilling breaker. *J. Fluid Mech.* **63**, 1–20.

[22] Lin, J.–C., Rockwell, D. 1994 Instantaneous structure of a breaking wave. *Phys. Fluids* **6**, 2877–2879.

[23] Nadaoka, K., Hino, M. & Koyano Y. 1989 Structure of the turbulent flow field under breaking waves in the surf zone. *J. Fluid Mech.* **204**, 359–387.

[24] Nessyahu, H. & Tadmor, E. 1990 Non-oscillatory central differencing schemes for hyperbolic conservation laws. *J. Comp. Phys.* **87**, 408–463.

[25] Richard, G. L. & Gavrilyuk, S. L. 2012 A new model of roll waves: comparison with Brock's experiments. *J. Fluid Mech.* **698**, 374–405.

[26] Richard, G. L. & Gavrilyuk, S. L. 2013 The classical hydraulic jump in a model of shear shallow water flows. *J. Fluid Mech.* **725**, 492–521.

[27] Richard, G. L. & Gavrilyuk, S. L. 2015 Modelling turbulence generation in solitary waves on shear shallow water flows. *J. Fluid Mech.* **698**, 374–405.

[28] Russo, G. 2005 Central schemes for conservation laws with application to shallow water equations, in *Trends and Applications of Mathematics to Mechanics* (S. Rionero and G. Romano, Eds.), pp. 225–246, Springer-Verlag Italia.

[29] Serre, F. 1953 Contribution à l'étude des écoulements permanents et variables dasn les cannaux. *Houille Blanche.* **8** (3), 374–388.

[30] Soares-Frazão, S. & Zech, Y. 2002. Undular bores and secondary waves – Experiments and hybrid finite-volume modeling. *J. Hydraulic Res.* **40** (1), 33–43.

[31] Soares-Frazão, S. & Guinot, V. 2008 A second-order semi-implicit hybrid scheme for one-dimensional Boussinesq-type waves in rectangular channels. *Int. J. Numer. Meth. Fluids* **58** (3), 237–261.

[32] Su, C. H. & Gardner, C. S. 1969 Korteweg - de Vries Equation and Generalisations. III. Derivation of the Korteweg - de Vries Equation and Burgers Equation *J. Math. Physics* **10**, 536–539.

[33] Teshukov, V. M. 2007 Gas-dynamics analogy for vortex free-boundary flows. *J. Appl. Mech. Tech. Phys.* **48** (3), 303–309.

[34] Tissier, M., Bonneton, P., Marche, F., Chazel, F. & Lannes, D, 2011 Nearshore dynamics of tsunami-like undular bore using a fully nonlinear Boussinesq model. *J. Coastal Res.* SI 64 (Proceedings of the 11th International Coastal Symposium), 603–607.

[35] Townsend, A. A. 1956 The structure of turbulent shear flow, Cambridge University Press.

[36] Treske, A. 1994 Undular bores (Favre-waves) in open channels: experimental studies. *J. Hydraulic Res.* **32** (3), 355–370.

6 Appendix A

The system describing the lower layer is :

$$\frac{\partial h}{\partial t} + \frac{\partial}{\partial x}\left(hU\right) = -M,$$

$$\frac{\partial}{\partial t}(hU) + \frac{\partial}{\partial x}\big(hU^2 + P\big) = p\big|_{z=h}\, h_x - M\, u\big|_{z=h},$$

$$\frac{\partial}{\partial t}\left(h\left(\frac{U^2}{2} + \varepsilon^2\frac{U_x^2}{6}h^2 + \frac{h}{2}\right)\right) + \frac{\partial}{\partial x}\left(hU\left(\frac{U^2}{2} + \varepsilon^2\frac{U_x^2}{6}h^2 + \frac{h}{2}\right) + UP\right)$$

$$= -p\big|_{z=h}(h_t + M) - M\left(\frac{u^2}{2} + \varepsilon^2\frac{U_x^2h^2}{2} + h\right)\Big|_{z=h},$$

where

$$P = \int_0^h p\, dz = p\big|_{z=h}\, h + \frac{h^2}{2} - \varepsilon^2\frac{h^3}{3}\big(U_{xt} + UU_{xx} - U_x^2\big).$$

The momentum equation is equivalent to

$$h\frac{DU}{Dt} + P_x = p\big|_{z=h}\, h_x - M\left(u\big|_{z=h} - U\right),$$

Developing the energy equation we have

$$h\frac{D}{Dt}\left(\frac{U^2}{2} + \varepsilon^2\frac{U_x^2}{6}h^2 + \frac{h}{2}\right) - M\left(\frac{U^2}{2} + \varepsilon^2\frac{U_x^2h^2}{6} + \frac{h}{2}\right) + U_xP + P_xU$$

$$= -p\big|_{z=h}\left(h_t + M\right) - M\left(\frac{u^2}{2} + \varepsilon^2\frac{U_x^2h^2}{2} + h\right)\Big|_{z=h}.$$

Using the momentum equation we can simplify the energy equation

$$h\frac{D}{Dt}\left(\varepsilon^2\frac{U_x^2}{6}h^2\right) + M\left(\frac{1}{2}\big(U - u\big|_{z=h}\big)^2 + \varepsilon^2\frac{U_x^2h^2}{3}\right)$$

$$-U_x\left(\varepsilon^2\frac{h^3}{3}\big(U_{xt} + UU_{xx} - U_x^2\big)\right) = 0.$$

Or

$$\varepsilon^2\frac{U_x^2h^2}{3}\frac{Dh}{Dt}h^2 + M\left(\frac{1}{2}\big(U - u\big|_{z=h}\big)^2 + \varepsilon^2\frac{U_x^2h^2}{3}\right) + hU_x\varepsilon^2\frac{U_x^2h^2}{3} = 0.$$

It implies

$$M\big(U - u\big|_{z=h}\big)^2 = 0.$$

Or

$$u\big|_{z=h} = U.$$

7 Appendix B

We replace the momentum equation for the lower layer by an equivalent one :

$$h\frac{DU}{Dt} + hh_x + h\eta_x - \varepsilon^2\left(\frac{h^3}{3}\big(U_{xt} + UU_{xx} - U_x^2\big)\right)_x = 0.$$

It can be transformed to :

$$U_t + \left(\frac{U^2}{2} + h + \eta\right)_x$$

$$-\varepsilon^2\left(hh_x\left(U_{xt} + UU_{xx} - U_x^2\right) + \frac{h^2}{3}\left(U_{xxt} + UU_{xxx} - U_xU_{xx}\right)\right) = 0.$$

It is equivalent to :

$$U_t + \left(\frac{U^2}{2} + h + \eta\right)_x$$

$$-\varepsilon^2\left(hh_xU_{xt} + \frac{h^2}{3}U_{xxt} + hh_x\left(UU_{xx} - U_x^2\right) + \frac{h^2}{3}\left(UU_{xxx} - U_xU_{xx}\right)\right) = 0.$$

It implies :

$$K_t + \left(\frac{U^2}{2} + h + \eta\right)_x$$

$$-\varepsilon^2\Big(hh_x\big(UU_{xx} - U_x^2\big) + \frac{h^2}{3}(UU_{xxx} - U_xU_{xx}) - U_xh_th_x - U_xhh_{tx} - \frac{2}{3}hh_tU_{xx}\Big) = 0.$$

Replacing h_t by

$$h_t = -(hU)_x - M$$

we obtain :

$$K_t + \left(\frac{U^2}{2} + h + \eta\right)_x$$

$$-\varepsilon^2\Big(U_xh_x\big(M + (hU)_x\big) + U_xh\big(M + (hU)_x\big)_x + \frac{2}{3}h\big(M + (hU)_x\big)U_{xx}$$

$$+hh_x\big(UU_{xx} - U_x^2\big) + \frac{h^2}{3}\big(UU_{xxx} - U_xU_{xx}\big)\Big) = 0.$$

It yields :

$$K_t + \left(\frac{U^2}{2} + h + \eta\right)_x - \varepsilon^2\Big(U_xh_x(hU)_x$$

$$+U_xh(hU)_{xx} + \frac{2}{3}h(hU)_xU_{xx} + hh_x\big(UU_{xx} - U_x^2\big) + \frac{h^2}{3}(UU_{xxx} - U_xU_{xx})\Big)$$

$$-\varepsilon^2\left(\frac{2}{3}(U_xhM)_x + \frac{1}{3}U_x(hM)_x\right) = 0.$$

Or

$$K_t + \left(\frac{U^2}{2} + h + \eta - \varepsilon^2 \frac{2}{3} hMU_x\right)_x - \varepsilon^2 \Big(U_x h_x (hU)_x + U_x h (hU)_{xx}$$

$$+ \frac{2}{3} h (hU)_x U_{xx} + h h_x \big(U U_{xx} - U_x^2\big) + \frac{h^2}{3} (U U_{xxx} - U_x U_{xx}) \Big) = \frac{\varepsilon^2}{3} U_x (hM)_x.$$

It can be simplified as :

$$K_t + \left(\frac{U^2}{2} + h + \eta - \frac{\varepsilon^2}{3h} \big(h^3 U_x\big)_x U - \frac{\varepsilon^2}{2} U_x^2 h^2 - \varepsilon^2 \frac{2}{3} hMU_x\right)_x = \frac{\varepsilon^2}{3} U_x (hM)_x.$$

One can transform the flux to obtain :

$$K_t + \left(KU + h + \eta - \frac{U^2}{2} - \frac{\varepsilon^2}{2} U_x^2 h^2 - \varepsilon^2 \frac{2}{3} hMU_x\right)_x = \frac{\varepsilon^2}{3} U_x (hM)_x.$$

An equivalent form is :

$$K_t + \left(KU + h + \eta - \frac{U^2}{2} - \frac{\varepsilon^2}{2} U_x^2 h^2 - \varepsilon^2 hMU_x\right)_x = -\frac{\varepsilon^2}{3} U_{xx} hM.$$

From the definition of K we have

$$K = U - \varepsilon^2 \frac{h^2}{3} U_{xx} - \varepsilon^2 h h_x U_x.$$

It allows us to eliminate U_{xx} as a function of K and U_x:

$$\varepsilon^2 U_{xx} = \frac{3}{h^2} \big(U - K - \varepsilon^2 h h_x U_x\big).$$

The derivative U_x is continuous at the jump, so the right-hand side of the equation for K is now well defined. An equivalent form is :

$$K_t + \left(KU + h + \eta - \frac{U^2}{2} - \frac{\varepsilon^2}{2} U_x^2 h^2 - \varepsilon^2 hMU_x\right)_x = -\frac{\varepsilon^2}{3} hMU_{xx}$$

$$= M \left(\frac{K - U}{h} + \varepsilon^2 h_x U_x\right).$$